


Causal pathways linking different flavours of ENSO with the Greater Horn of Africa short rains

David MacLeod^{1,2}  | Richard Graham³ | Chris O'Reilly¹ | George Otieno⁴ | Martin Todd⁵

¹Atmospheric Oceanic and Planetary Physics, Department of Physics, University of Oxford, UK

²School of Geographical Sciences, University of Bristol, Bristol, UK

³Met Office, Exeter, UK

⁴IGAD Climate Prediction and Application Centre (ICPAC), Ngong Town Kibiku A Road, Nairobi, Kenya

⁵Department of Geography, University of Sussex, Brighton, UK

Correspondence

David MacLeod, School of Geographical Sciences, University of Bristol, Bristol BS8 1SS, UK.

Email: david.macleod@bristol.ac.uk

Funding information

Science for Humanitarian Emergencies and Resilience (SHEAR), Grant/Award Numbers: NE/P000428/1, NE/P000568/1, NE/P000673/1; UK Natural Environment Research Council; Economic and Social Research Council; UK Department for International Development

Abstract

There is a strong association between canonical El Niño and a wet Greater Horn of Africa (GHA) short rains. However, the link with Modoki El Niño events appears to be significantly weaker. In order to understand this, we present an analysis of observational data and idealised climate model experiments. Idealised atmospheric simulations isolate the direct influence of Pacific heating on the GHA and reveal that neither the longitudinal position nor the observed weaker magnitude of Modoki Pacific heating anomalies can explain the difference in teleconnections. The direct effect of canonical or Modoki Pacific heating patterns on the GHA is similar and neither reproduces the structure of the full GHA teleconnection: they both generate a wet-dry dipole over the GHA instead of large-scale single-signed wet anomalies. Our results indicate that the strong canonical ENSO influence on GHA is indirect, mediated through its strong relationship with the Indian Ocean Dipole (IOD). By contrast, Modoki ENSO is uncorrelated with the IOD, resulting in weak teleconnection to GHA. Understanding these differences aids seasonal forecast interpretation, whilst their representation in models is likely a prerequisite for making accurate projections of changes in extremes over the GHA and beyond.

KEYWORDS

ENSO, Greater Horn of Africa, IOD, seasonal forecasting

1 | INTRODUCTION

The climate of the Greater Horn of Africa (GHA) is highly variable and the region is frequently affected by significant large scale seasonal flooding and drought (Mwangi *et al.*, 2013; Kilavi *et al.*, 2018). The GHA short rains from October to December show particularly large interannual variability with high predictability due to a

strong teleconnection to El Niño Southern Oscillation (ENSO) and the Indian Ocean Dipole (IOD) (Saji *et al.*, 1999; Nicholson, 2017). The IOD in particular has been identified as the key driver of the short rains, whilst it has been suggested that teleconnections from the tropical Pacific only impact the GHA indirectly (Rocha and Simmonds, 1997; Goddard and Graham, 1999; Latif *et al.*, 1999; Bahaga *et al.*, 2019).

This is an open access article under the terms of the Creative Commons Attribution License, which permits use, distribution and reproduction in any medium, provided the original work is properly cited.

© 2020 The Authors. *Atmospheric Science Letters* published by John Wiley & Sons Ltd on behalf of Royal Meteorological Society.

This high predictability has led to the development of early anticipatory actions to manage climate variability and efforts in GHA have been based on ENSO forecasts alone (de la Poterie *et al.*, 2018). However, ENSO events vary in their character: anomalous sea surface temperature (SST) in the east Pacific is associated with El Niño events and has long been studied (as such is referred to as ‘canonical’ ENSO). More recently a different flavour of ENSO has been identified, when SST anomalies are located in the central Pacific Ocean, sandwiched by cold SSTs over the tropical eastern and western Pacific Ocean Ashok *et al.* (2007). This kind of ENSO event is known as ENSO ‘Modoki’.

Current understanding identifies a distribution of ENSO types, of which East and Central Pacific flavours (canonical and Modoki) capture the extrema, and some events do not clearly exist as one type or the other (Capotondi *et al.*, 2015) although the idea of two types is useful as a framework to understand variability in ENSO teleconnections, and are commonly considered in operational seasonal forecasting and the academic literature (Yeh *et al.*, 2018). However despite their prevalence, there are large uncertainties concerning the precise nature of regional ENSO precipitation and temperature teleconnections between different types of events (WMO, 2020).

In particular the differential impact of ENSO variability on the short rains of GHA is unclear; Ashok *et al.* (2007) suggest no strong link between Modoki El Niño and GHA rainfall, whilst (Preethi *et al.*, 2015) indicate an anticorrelation over inland areas. This suggests that anticipatory action which does not distinguish between ENSO flavours may lead to significant operational errors. In order to support accurate forecast-based preparedness, we evaluate observational data and use climate model experiments, in order to diagnose the differential GHA rainfall responses to the different ‘flavours’ of ENSO.

2 | OBSERVATIONS AND HYPOTHESISED CAUSAL PATHWAYS

Indices of canonical ENSO (Niño 3.4, hereafter N34), and the IOD were obtained from the National Oceanic and Atmospheric Administration (NOAA) and the ENSO Modoki Index (EMI, defined in Ashok *et al.* (2007)) was obtained from the Japan Agency for Marine-Earth Science and Technology (JAMSTEC; please see acknowledgments for web addresses of these data products). CHIRPS (Funk *et al.*, 2015) at 0.025° resolution was used to evaluate spatial details of rainfall over land, whilst

GPCP (Adler *et al.*, 2003) at 2.5° is used for evaluating large-scale signals. ERA5 reanalysis is used to evaluate atmospheric circulation (ECMWF, 2019). For all analysis, October–December (OND) averages/totals are shown, and data is evaluated over the period 1981–2017.

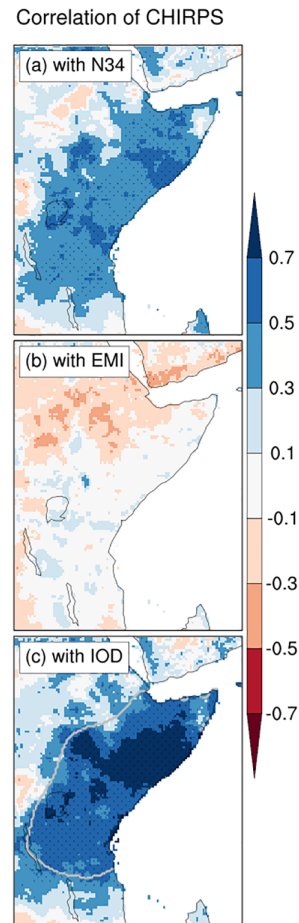
Analysis of large-scale climate indices with GHA rainfall leads to a set of hypothesised causal pathways (Figure 1). OND rainfall correlates very strongly with the IOD and strongly with N34 consistent with (Nicholson, 2017). However we find no strong correlation against the EMI. This is consistent with previous work which finds no strong precipitation signal in the western Indian Ocean during Modoki events occurring in boreal winter (Ashok *et al.*, 2007). Preethi *et al.* (2015) note negative correlations of the short rains with EMI across large regions of inland GHA northwards of Lake Victoria to the coast, after filtering out other influences. This is somewhat consistent with Figure 1b showing negative correlation in the north of the region. Differences may be related to the different periods under study (Preethi *et al.* (2015) consider data only up to 2010) and the use of partial versus full correlations. We also note significant correlation between N34 and EMI; this reflects the continuous nature of ENSO diversity (Capotondi *et al.*, 2015) as there is some co-variation in the indices: events with warming present across the East and Central Pacific will be classified as with both positive N34 and EMI indices. However the distinction arises from events which show cooling in the East Pacific alongside warming in the Central Pacific; these will be classified with a strong EMI, with neutral (or even weakly negative N34) index.

Correlating these indices directly with each other (Figure 1d) shows a strong relationship between N34 and IOD, consistent with previous work showing that El Niño events predispose the Indian Ocean to strong positive IOD events (Black *et al.*, 2003). No statistically significant correlation is found at the 5% level between the EMI and IOD, consistent with Ashok *et al.* (2007).

This analysis leads us to the hypothesised causal networks outlined in Figure 1e. We then use climate model experiments to test:

1. Direct links between the Pacific and the GHA, unmediated by the Indian Ocean, that is, do causal mechanisms A and B exist? We compare the relative size of A and B and use idealised and composite-SST forced experiments to find out if differences in longitudinal location, or the relative magnitude of Pacific SST anomalies can explain the observed differences in the canonical and Modoki teleconnections.
2. How important is any direct influence of ENSO on GHA rainfall relative to that mediated by IOD. That is, how large is A relative to C? This is approached

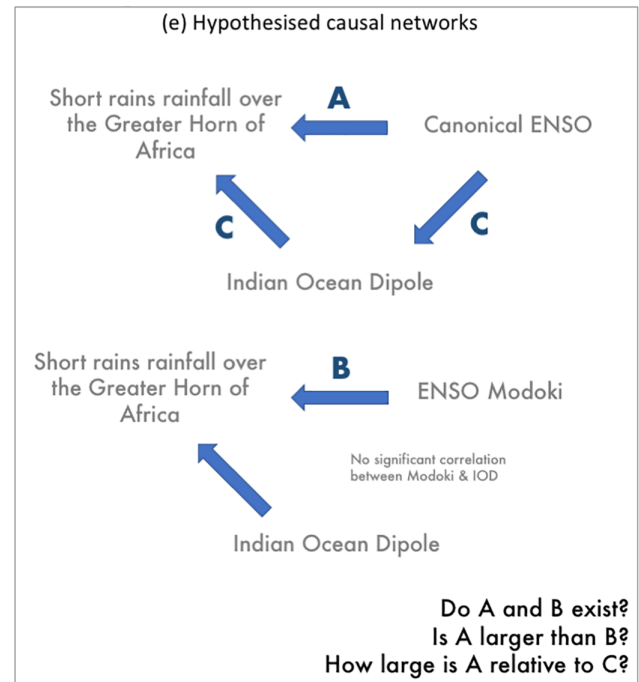
FIGURE 1 Observed correlation of October–December CHIRPS rainfall 1981–2017 over the GHA with (a) Niño 3.4 (b) ENSO Modoki and (c) IOD: Correlations with stippling exceed a 99% statistical significance level calculated with a *t*-test. (d) Shows cross-correlations between the climate indices along with an index of short rains (SR) rainfall, defined as the average over the domain indicated by the grey line in (c), with correlations significant at the 99% level indicated with asterisks. (e) Shows hypothesised causal links along with a summary of specific research questions



(d) Cross-correlations between all indices

	N34	EMI	IOD
EMI	0.60*		
IOD	0.65*	0.17	
SR	0.52*	0.01	0.77*

(e) Hypothesised causal networks



through analysis of composites of observed rainfall and circulation during ENSO events and corresponding responses in forced SST experiments. We address warm and cold events separately, to disentangle any asymmetric response to El Niño/ La Niña.

3 | CLIMATE MODEL EXPERIMENTS

Atmospheric model simulations with prescribed lower boundary conditions are run to investigate the sensitivity of the short rains to characteristics of the SST forcing. We use the ECMWF Integrated Forecasting System (IFS), cycle CY41R1 at T255 resolution (around 80 km the equator). Our control experiment consists of a 37-member ensemble of atmospheric simulations, initialised on 1-September for each year 1981–2017 to account for variability related to the initial state: the ensemble mean is shown for all results to extract the forced signal. All simulations run through to the end of December and use a smoothed daily climatology (1981–2017) from HadISST as a lower boundary condition (Rayner *et al.*, 2003).

Six idealised experiments are run based on the control setup, using the same 37 set of initial conditions. For each, a constant 1 K anomaly was added to the climatological SST forcing in the eastern, central or west Pacific using both negative anomalies (experiments EP – 1, CP – 1 and WP – 1) and positive anomalies (EP + 1, CP + 1 and WP + 1). The location of SST forcing is indicated with contours in Figure 2 whilst the full SST field is shown in Figure S1. A uniform one degree anomaly in each of these areas is not intended to be realistic, however these idealised experiments isolate the impact of the longitudinal position of heating alone.

We next run six experiments using realistic SST forcing. The forcing is generated by first identifying 5 years each with observed East/Central Pacific El Niño/La Niña conditions (EPEN, CPEN, EPLN, CPLN). Observed daily SST anomalies are constructed for each of the 5 years and used to create forcing for each case by adding the composited anomalies in the Pacific region to the baseline HadISST1 daily climatology. For the EPEN case, three forcing fields are constructed: one that isolates the Pacific anomaly (EPEN) one that isolates the Indian Ocean anomaly (IODA) and one that includes all tropical

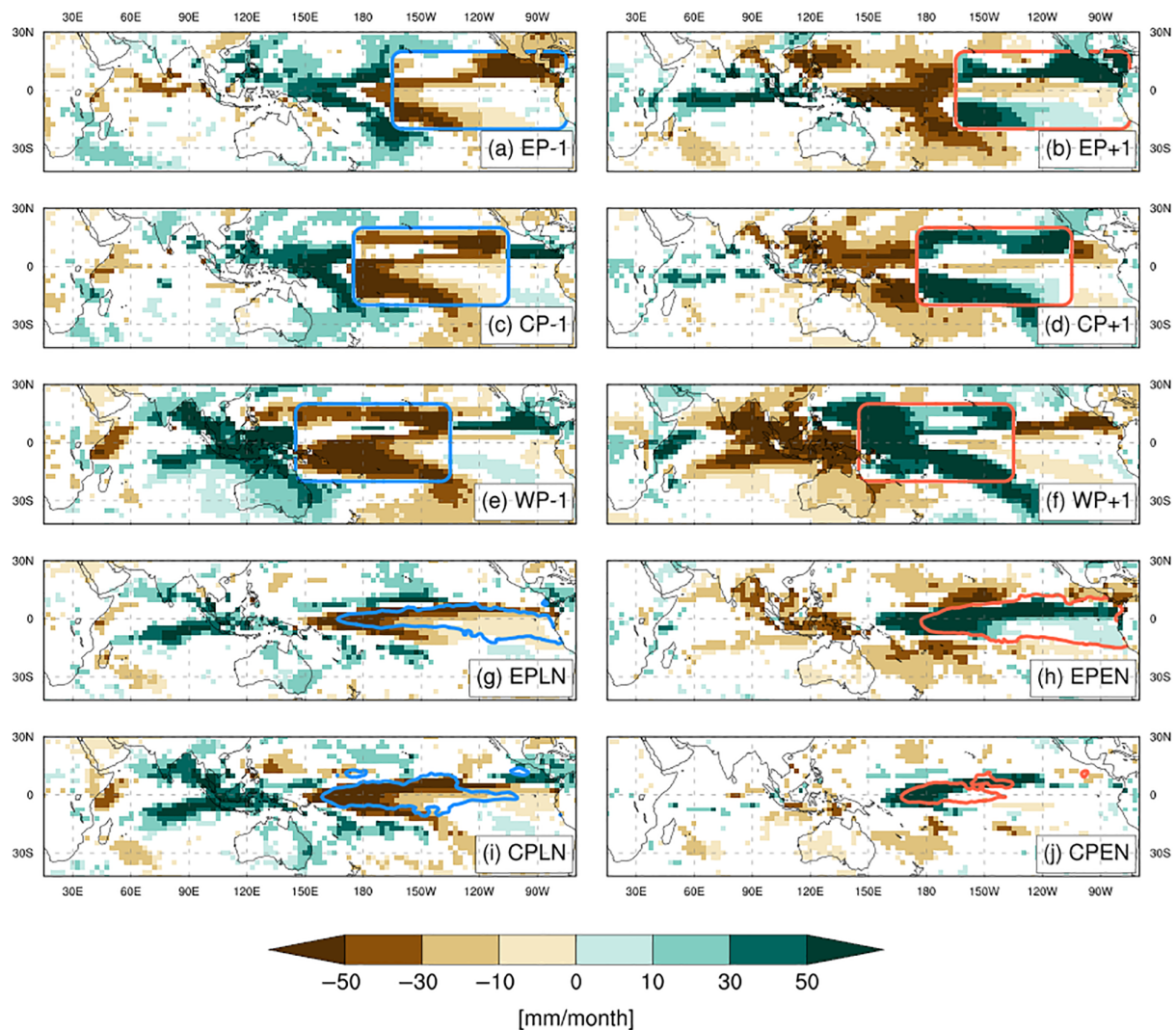


FIGURE 2 Impacts on precipitation from all experiments; differences minus control. Differences falling below a 90% significance level according to a t-test are masked. Red (blue) contours indicate SST forcing anomalies greater (less than) 0.5 K (-0.5 K)

anomalies (TPIO). Full details of the methodology are provided in Supporting Information.

We note that the selection of 5 years to define the composite pattern is not meant to be definitive; there exist more than one method of categorising ENSO types and these do not always agree (Yu *et al.*, 2012). For our purposes here we only require that the resultant SST anomaly is consistent with that seen in typical eastern or central Pacific events. A comparison of Figure 2 and Figure S1 with results of Yu *et al.* (2012); Capotondi *et al.* (2015) shows that this requirement is met. In addition whilst we note the spectrum of ENSO diversity (Yu *et al.*, 2012), we also note that canonical and Modoki are prominent in the observational record, and the concepts play a key role in the operational seasonal forecasting community. We thus aim to understand the impacts of these archetypal flavours.

By applying anomalous forcing in the Pacific sector alone, experiments estimate the direct forcing effect by blocking off any indirect causal pathway through Pacific-driven Indian Ocean variability. Results of these composite-forced experiments can then be compared with the corresponding composites of observations to indicate the degree to which Pacific forcing in isolation is responsible for the observed response over GHA.

4 | RESULTS

Idealised heating in the Pacific produces a wet response over GHA (e.g., Figure 2b), whilst cooling produces a small drying effect, centred off-coast (Figure 2a). This suggests that there is a direct link between the Pacific and GHA unmediated by the Indian Ocean; that the link

A in Figure 1e exists. Moving the heating/cooling into the central and west Pacific does not reduce the magnitude of this GHA response for cooling events, although the wet response of CP + 1 (Figure 2d) is slightly weaker over GHA than EP + 1 (Figure 2b). However the experiments with forcing located in the far west Pacific (WP - 1 and WP + 1, Figure 2e-f) show the largest precipitation response across the combined GHA and West Indian Ocean sector. Precipitation anomalies over GHA during the short rains are linked to the Indian Ocean Walker Circulation (IOWC) and the impact of EP and CP experiments on the upper and lower branches of the IOWC is minimal (Figures S2 and S3). On the other hand a large impact on the IOWC is seen for the WP experiments, which is consistent with the large precipitation response seen for experiments WP + 1 and WP - 1. This suggests that the further-west longitudinal position of SST anomalies cannot explain the observed weaker impact of Modoki ENSO over GHA.

Considering the more realistic heating experiments, EPEN (Figure 2h) shows a wet signal off the GHA coast, some wet over land near the coast and a dry signal inland to the east of Lake Victoria. The CPEN experiment by contrast shows no statistically significant precipitation response over GHA (Figure 2j). As such, for warm phases of ENSO the link A has slightly larger magnitude than link B. Cooling experiments show the opposite result, with GHA drying signals that are stronger and more widespread in CPLN (Figure 2i), whilst EPLN shows no significant dry response over GHA land, although a similar strength but opposite-signed impact to EPEN is seen off the coast (Figure 2g). This suggests that for cold ENSO phases the link B has slightly larger magnitude than link A. This is reflected in the circulation fields, where CPLN shows a greater perturbation of the IOWC than EPLN, whilst CPEN shows no impact on the IOWC (Figures S2g-j and S3g-j).

This forced response of GHA precipitation to East Pacific warming is much smaller than the observed response (Figure 3a,e); the direct response alone is insufficient to reproduce the full teleconnection. Further, the spatial structure differs markedly; the observed composites show a widespread wet signal extending from the western Indian Ocean across GHA, whilst simulations show a similar wet response east of 40°E but with weaker anomalies over the GHA coast and an opposing dry signal around Lake Victoria. The respective circulation anomalies are instructive. Both observations and the EPEN experiment show a weakening or reversal of the IOWC over most of the Indian Ocean that is, large easterly zonal wind anomalies at the surface (Figure 3i,m) and westerlies in the upper troposphere (Figure S4a,e). West of 60°E including the GHA itself, however, westerly

near-surface anomalies are evident in observations (Figure 3m) but not reproduced by the forced experiment, which has near-surface easterly anomalies across the entire Indian Ocean and GHA. For Modoki warming, the simulated (CPEN) and observed precipitation responses are more similar, with wet anomalies over the Indian Ocean and coast of GHA and a dry signal seen inland (Figures 3b,f).

Both canonical and Modoki La Niña observed composites show a drying over the western Indian ocean and GHA, with larger magnitudes for Modoki events (Figure 3g, h). The simulations are largely able to reproduce the signal east of 40°E (Figure 3c, d). However, similar to heating events, the sign of the impacts diverge inland over GHA: observed composites show a uniform dry signal from the ocean through to the interior of GHA (Figure 3g,h) with a sign change in zonal wind anomalies from westerlies east of 60°E to easterlies over the coast (Figure 3o,p). By contrast, simulations show westerly anomalies stretching into the interior of the continent (Figure 3k,l), along with a dry response centred off the coast and a wet response inland (Figure 3c,d).

Finally, the relative roles of the Indian and Pacific Oceans during canonical El Niño years are evaluated by comparing experiments TPIO, IODA with Pacific-only EPEN (Figure 4). Experiments TPIO and IODA both reproduce the same wet signal over the GHA, co-located with strong positive anomalies in 200 mb divergence, whilst EPEN only produces a moderate wet signal, accompanied by a slight reduction in 200 mb divergence. This suggests that the direct effect of El Niño then actually leads to increased subsidence over GHA and that any increases in rainfall originate at lower levels through circulation-driven increases in surface convergence rather than deep convection. Conversely, local warming linked to the IOD increases divergence at the top of the atmosphere, suggesting deep convection. Returning to the causal pathways in Figure 1e, this suggests that the majority of the overall canonical ENSO teleconnection arises from pathway C – indirectly via the IOD – and the magnitude of pathway A is small relative to C.

Differences in the structure of low level zonal wind anomalies are revealing. EPEN shows unrealistic uniform easterlies across both land and ocean. TPIO shows strong easterlies across the Indian Ocean, met by westerlies over GHA. For IODA the structure is similar but the westerlies from GHA are much stronger and extend further into the Indian Ocean to 60°E. This suggests during canonical El Niño events the direct and indirect influences on near-surface zonal winds near GHA is opposite: the direct effect promotes easterlies, whilst the indirect effect promotes westerlies. The total impact is therefore a combined result of contrary influences directly from the

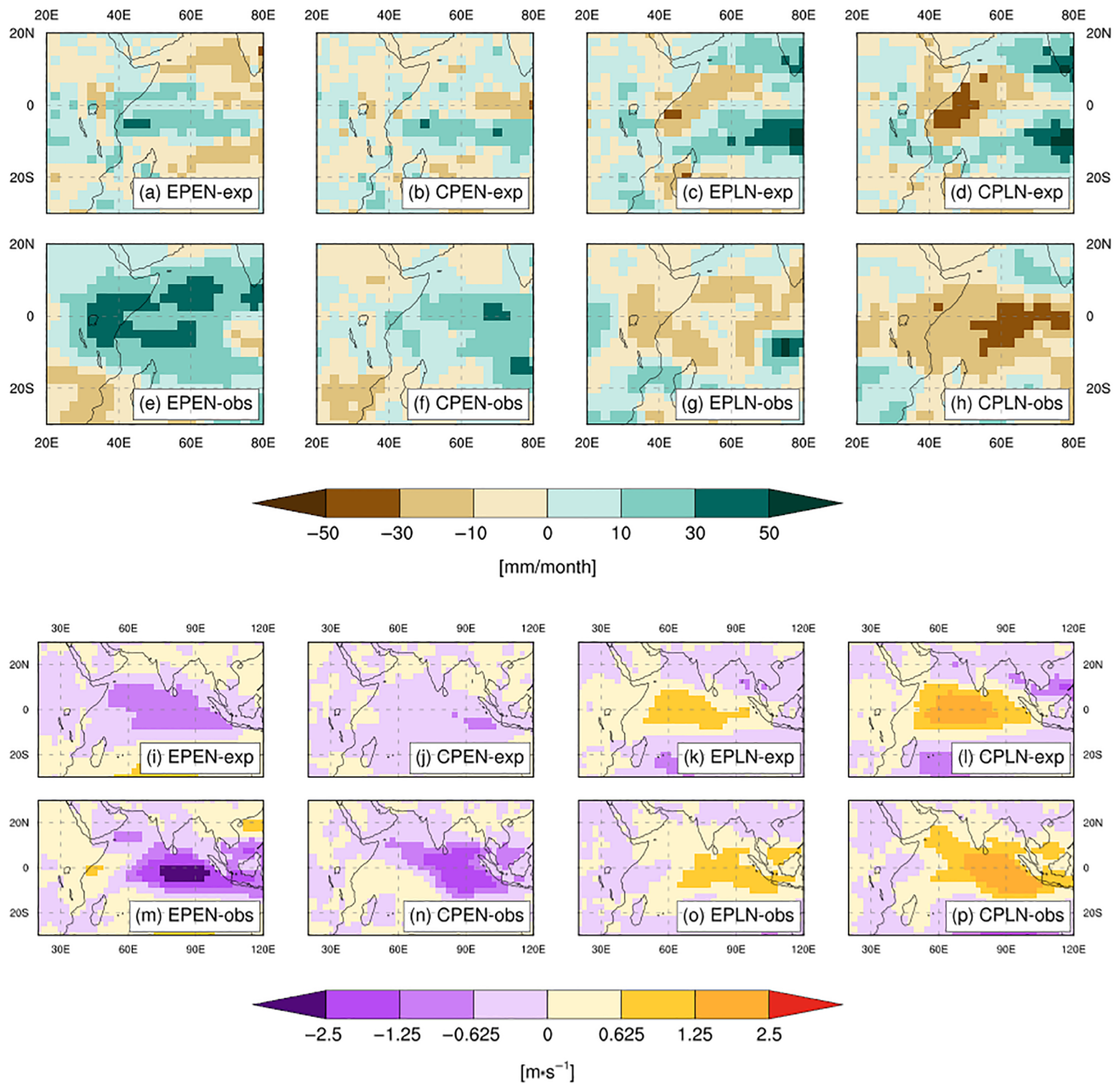


FIGURE 3 Comparison of the response to composite-forced SST experiments with the observed response from ENSO composites. (a–d) Show the difference of OND precipitation in experiments against control and (e–h) show observed precipitation anomalies in composited EPEN, CPEN, EPLN and CPLN years. (i–p) as (a–h) but for zonal wind at 1,000 mb. For clarity no significance masking is applied; the differing methodology of experiments and composites results in different threshold criteria for considering results significant

Pacific and Indian Oceans. We note that the observed low level wind structure is most faithfully represented in IODA (compare Figures 3m and 4c). However, when the Pacific forcing is included (Figure 4c, TPIO), the easterly influence dominates over the west Indian Ocean, with westerly anomalies confined to the continent. This suggests that in this model, the direct influence of the Pacific Ocean on the atmospheric circulation may be too strong relative to the direct forcing from the Indian Ocean.

5 | CONCLUSIONS

In this work we have used a set of idealised model experiments along with analysis of observations to evaluate causal pathways linking GHA rainfall to variability in the Pacific and Indian Oceans. A small direct effect of Pacific SST variability is found (i.e., pathways A & B in Figure 1e exist). Uniform Pacific heating (cooling) generates wet (dry) anomalies in the west Indian Ocean and over the

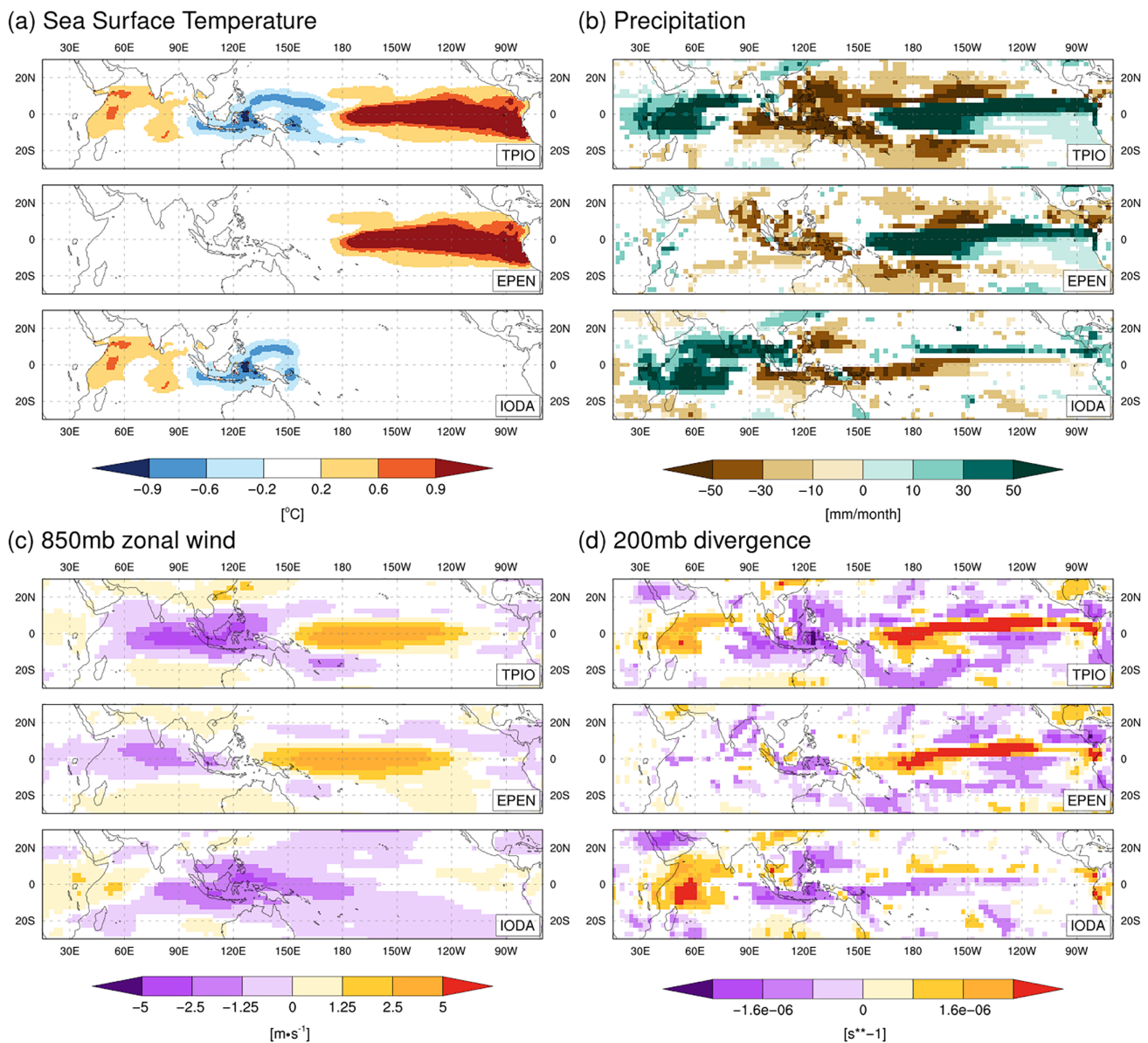


FIGURE 4 Comparing the direct role of Pacific and Indian Ocean SST during canonical El Niño years. (a) Shows SST forcing in three experiments: For each, anomalies are generated from composited EPEN years but applied across the tropical Pacific and Indian Ocean (TPIO), the East Pacific (EPEN, as previous) and the IOD dipole (IODA). (b-d) Respectively show the anomalous responses of precipitation, 850 mb zonal wind and 200 mb divergence. Differences below a 90% significance level according to a t-test are masked

GHA, which are larger when forcing is located further west in the Pacific. This demonstrates that the weaker observed Modoki teleconnection to GHA is not a direct effect of the longitudinal position of Pacific heating. However when realistic El Niño heating anomalies are imposed, pathway A is indeed larger than B for positive ENSO phases, likely attributed to the lower magnitude of SST anomalies in the central Pacific compared to the east. Conversely, with realistic Pacific cooling imposed in which the SST anomalies of Modoki and canonical La Niña, are of similar magnitude, GHA drying is stronger in the former case (i.e., pathway A is smaller than B for

negative ENSO phases), suggesting greater sensitivity to west Pacific SST anomalies. It is notable that Pacific cooling alone, without the Indian Ocean, is sufficient to reproduce the magnitude of the observed drying response over the GHA coast.

Circulation and rainfall responses in forced Pacific-only SST experiments show important differences to the observed teleconnections. In observed composites of canonical El Niño events a large uniform wet signal is seen across the GHA associated with zonal wind anomalies of opposite-sign east and west of 60°E. By contrast experiments with Pacific forcing alone show a wet-dry

dipole over the GHA, with drying around Lake Victoria and a wet response over the coast, whilst zonal winds show uniform easterly anomalies across GHA and the Indian Ocean. Similar (but opposite) responses are seen for Pacific-only cooling events. These differences in the teleconnections between observations and the Pacific-only experiments are then related to SST anomalies in both the west and east Indian Ocean which act to modify the direct Pacific effect (notably two additional experiments isolating the impact of each IOD pole show comparable impacts on GHA rainfall, in both cases significantly larger than EPEN, not shown). For positive IOD events, locally warm SST increases upward motion throughout the atmosphere, favouring deep convection and westerlies over GHA. Without anomalous SSTs in the Indian Ocean easterly zonal wind anomalies can extend all the way into the GHA interior. Concurrently, the cold eastern pole of the IOD will suppress convection there and weaken the IOWC and increase convection in the west which will also act to limit the incursion of the direct-ENSO related easterlies into Africa. These results explain the findings of Goddard and Graham (1999), who also note that Pacific forcing may act to counteract the effect of Indian Ocean on GHA. These competing effects of Pacific and Indian Ocean variability on GHA rainfall are summarised in Figure 5.

We speculate that this extension of the large-scale near-surface easterlies across GHA with the direct Pacific effect could suppress inland rainfall around Lake Victoria through two mechanisms. Firstly it may impede westerly

wind incursions from the Congo, which have been associated with rainfall events (Finney *et al.*, 2019). Secondly they may enhance the low level Turkana Channel jet in northwest Kenya (Kinuthia, 1992; Nicholson, 2016), which may inhibit rainfall.

Indian Ocean forcing alone reproduces a GHA rainfall response more consistent with observations, both in the size of anomalies and spatial pattern. This suggests that the observed link between canonical El Niño and wet GHA short rains is largely mediated through the Indian Ocean through El Niño's conditioning of the Indian Ocean for positive IOD events (Black *et al.*, 2003). In other words, pathway A of Figure 1e is much smaller than pathway C. This result is consistent with recent significant short rains anomalies: in 1997 the very wet short rains was accompanied by both strong El Niño and positive IOD event (Latif *et al.*, 1999), whilst in 2015 the very strong El Niño event was only accompanied by a relatively modest positive IOD and led to lower-than-anticipated rainfall over the region (MacLeod and Caminade, 2019). Most recently, the recent 2019 short rains was one of the wettest on record and occurred in conjunction with a record-breaking IOD event, without any El Niño activity in the Pacific (Wainwright *et al.*, 2020).

The primacy of the IOD-mediated link found here is consistent with previous work highlighting Indian Ocean variability as a key driver of GHA rainfall (Rocha and Simmonds, 1997; Goddard and Graham, 1999; Latif *et al.*, 1999; Black *et al.*, 2003), and with statistical

ENSO impacts on the Greater Horn of Africa short rains

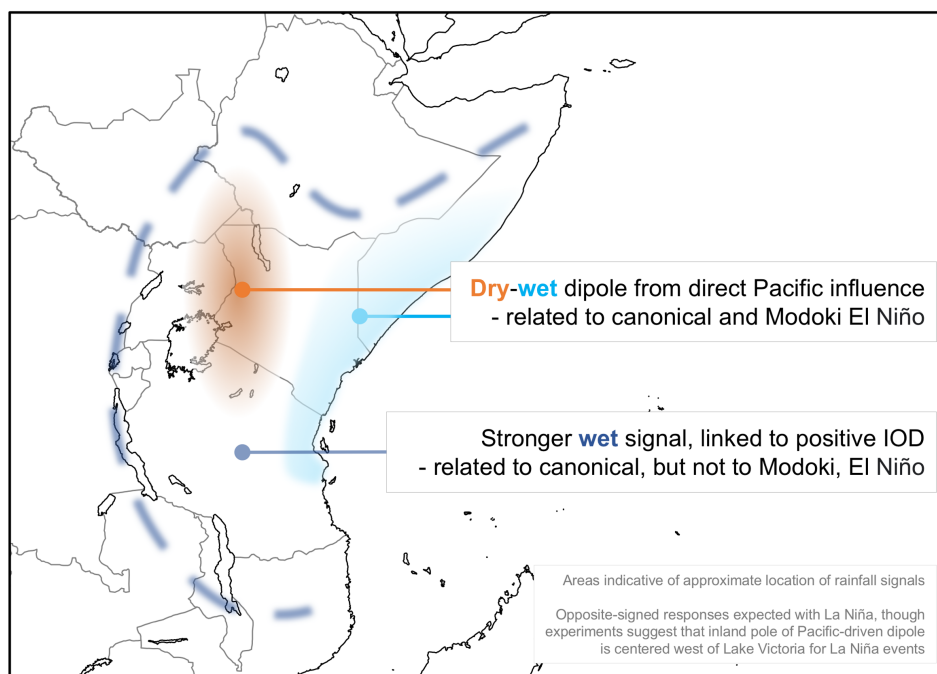


FIGURE 5 Summary schematic of the links between ENSO and GHA short rains rainfall

analysis of historical climate data which shows the influence of canonical ENSO to be mediated by in-phase occurrence of the IOD Bahaga *et al.* (2019). It is also consistent with the findings of Bahaga *et al.* (2015), who use a low resolution (3.75°) atmospheric model to isolate the effect of Indian Ocean SST variability on the short rains and conclude that SSTs outside the Indian Ocean play a minor role (we extend these findings by focusing on the comparative direct effects of canonical and Modoki ENSO). Our findings then lead to the conclusion that the weak observed teleconnection of the short rains with El Niño Modoki can be explained by lack of a strong correlation of Modoki El Niño with the IOD, which is seen here (Figure 1d) and in previous work (Ashok *et al.*, 2007). They also demonstrate that an analogue approach based purely on El Niño variability will likely lead to significant forecast errors, and Indian Ocean variability must be taken into account.

A strong test of the conclusions of Indian Ocean primacy would be the co-occurrence of opposite-signed anomalies in the Pacific and Indian Ocean. However instances of this type are rare: the only instance identified is during the short rains of 2011 which saw a relatively weak La Niña Modoki increasing in strength to the end of the year, alongside a positive IOD which returned to neutral by December. Rainfall anomalies for this season show strong positive anomalies for October and November, with neutral anomalies in December (not shown). This shows clearly the dominance of the positive IOD, despite the concurrent strong La Niña Modoki in the Pacific, and strongly supports our conclusions.

Our work has implications for understanding both climate projections and seasonal forecasting over GHA. The future of the IOD and climate extremes around the Indian Ocean rim may well be determined by the balance between various effects which have emerged from analysis of CMIP5 models, for example, increased susceptibility to extreme positive IOD and IOWC reversal events driven by heterogeneous Indian Ocean SST trends (Cai *et al.*, 2014), and reduced triggering of those reversals driven by a shift toward El Niño Modoki (Yeh *et al.*, 2009). However, we note that Cai *et al.* (2014) find the same level of correlation between IOD and both canonical and Modoki ENSO in most CMIP5 models, suggesting they are unable to discriminate the different Indian Ocean response to different modes of Pacific variability.

Analysis of seasonal forecasts from ECMWF also suggest flawed simulation of Indian Ocean responses to Pacific variability, where a too-strong positive IOD-like response is generated when the maxima of Pacific El Niño warming is located further west than normal (MacLeod, 2019). Many other dynamical seasonal forecast systems exhibit spatial variations in prediction skill that

reflect aspects of the dipole pattern of Figure 5 (Richard Graham, personal communication, see also Shukla *et al.* (2016); MacLeod (2019); Walker *et al.* (2019)), suggesting correct representation of the relative strengths of the direct and IOD-mediated responses are a key issue for model development. Work is in progress to investigate these issues to help inform the use of multi-model ensembles at ICPAC (George Otieno, personal communication).

Further, at least half of all CMIP5 models have worrying biases in the mean state including an incorrect sign of mean zonal winds over the Indian Ocean (Hirons and Turner, 2018) (also shown evolving rapidly in seasonal forecasts by Walker *et al.* (2019)). Such a mean state bias impacts the ability of models to generate credible teleconnection mechanisms as shown by Hirons and Turner (2018). There is, therefore, a critical need to improve our understanding and modelling of the triggering of IOD events and the weak Modoki ENSO-IOD link; both to determine how this may evolve as the background SST state warms differentially, and to ensure that seasonal forecasting models accurately represent the

TABLE 1 Archiving labels which can be used to access the data, stored at ECMWF MARS (see www.ecmwf.int for more details of access)

Experiment name	Archiving label
CTRL	B2B6
EP - 1	B2BB
EP + 1	B2BC
CP - 1	B2BF
CP + 1	B2BG
WP - 1	B2BJ
WP + 1	B2BK
EPLN	B2DZ
EPEN	B2DX
CPLN	B2E0
CPEN	B2DY
TPIO	B2EU
IODA	B2EV

TABLE 2 Years used to define OND composites for each type of ENSO event

Composite	Years
Canonical El Niño (EPEN)	1982, 1987, 1997, 2002, 2015
El Niño Modoki (CPEN)	1990, 1991, 1994, 2004, 2009
Canonical La Niña (EPLN)	1985, 1995, 1999, 2007, 2017
La Niña Modoki (CPLN)	1983, 1988, 1998, 2008, 2010

balance between predictable signals arising from the Pacific and the Indian Ocean.

ACKNOWLEDGEMENTS

We acknowledge ECMWF for provision of computing resources used to run experiments under a ‘Special Project’. Climate model data is archived at ECMWF, is accessible with a free licence, details can be found at www.ecmwf.int (archiving details of the experiments are provided in Table 1). We also acknowledge ECMWF for the use of ERA5 reanalysis data and the Climate Hazards Group of UCSB for CHIRPS data. N34 and IOD data was provided by NOAA, available at: https://www.esrl.noaa.gov/psd/gcos_wgsp/Timeseries/, whilst EMI data was downloaded from JAMSTEC and is available at: http://www.jamstec.go.jp/frsgc/research/d1/iod/modoki_home.html.en. This work was funded by the Science for Humanitarian Emergencies and Resilience (SHEAR) consortium project ‘Towards Forecast-based Preparedness Action’ (ForPac), grant numbers NE/P000673/1, NE/P000568/1 and NE/P000428/1. The SHEAR programme is funded by the UK Natural Environment Research Council, the Economic and Social Research Council and the UK Department for International Development.

CONFLICT OF INTEREST

The authors declare no potential conflict of interest.

FURTHER DETAILS OF COMPOSITE-FORCED CLIMATE MODEL EXPERIMENTS

Forced-SST experiments are run using realistic SST forcing derived from SST anomaly composites of the five largest years of canonical (Niño/La Niña, EPEN/EPLN) or Modoki Central Pacific El Niño/La Niña, CPEN/CPLN) events. To define the years, first October–December averages of both the Niño 3.4 index (N34) and ENSO Modoki Index (EMI, http://www.jamstec.go.jp/frsgc/research/d1/iod/modoki_home.html.en) are taken and standardised. (both indices are downloaded from NOAA (https://www.esrl.noaa.gov/psd/gcos_wgsp/Timeseries/)). Every year is then classified as follows:

- EPEN: if N34 is greater than zero and greater than the absolute value of EMI
- CPEN: if EMI is greater than zero and greater than the absolute value of N34
- EPLN: if N34 is below than zero and the absolute value is greater than the absolute value of EMI
- CPLN: if EMI is below than zero and the absolute value is greater than the absolute value of N34

The absolute value condition is included in order to catch strong canonical El Niño events which have a

negative EMI index and could appear as a moderate La Niña Modoki (for instance, 1997). Once all years have been calculated, for each category we pick the 5 years which have the highest or lowest respective index (i.e., N34 for EPEN/EPLN and EMI for CPEN/CPLN). The resulting years are shown in Table 2.

For each set of 5 years a composite daily anomaly SST field is calculated over the domain 20°N–20°S, 150°E–85°W, then added to the climatology field elsewhere with exponential smoothing over a 10° perimeter to avoid discontinuities. Only positive anomalies within the domain are added for El Niño experiments and only negative anomalies added for La Niña experiments.

ORCID

David MacLeod  <https://orcid.org/0000-0001-5504-6450>

REFERENCES

- Adler, R.F., Huffman, G.J., Chang, A., Ferraro, R., Xie, P.-P., Janowiak, J., Rudolf, B., Schneider, U., Curtis, S., Bolvin, D., Gruber, A., Susskind, J., Arkin, P. and Nelkin, E. (2003) The version-2 global precipitation climatology project (GPCP) monthly precipitation analysis (1979–present). *Journal of hydrometeorology*, 4, 1147–1167.
- Ashok, K., Behera, S.K., Rao, S.A., Weng, H. and Yamagata, T. (2007) El Niño Modoki and its possible teleconnection. *Journal of Geophysical Research: Oceans*, 112, C11007. <https://doi.org/10.1029/2006JC003798>.
- Bahaga, T., Mengistu Tsidu, G., Kucharski, F. and Diro, G. (2015) Potential predictability of the sea-surface temperature forced equatorial east African short rains interannual variability in the 20th century. *Quarterly Journal of the Royal Meteorological Society*, 141, 16–26.
- Bahaga, T.K., Fink, A.H. and Knippertz, P. (2019) Revisiting interannual to decadal teleconnections influencing seasonal rainfall in the greater horn of africa during the 20th century. *International Journal of Climatology*, 39, 2765–2785.
- Black, E., Slingo, J. and Sperber, K.R. (2003) An observational study of the relationship between excessively strong short rains in coastal East Africa and Indian Ocean SST. *Monthly Weather Review*, 131, 74–94.
- Cai, W., Santoso, A., Wang, G., Weller, E., Wu, L., Ashok, K., Masumoto, Y. and Yamagata, T. (2014) Increased frequency of extreme Indian Ocean dipole events due to greenhouse warming. *Nature*, 510, 254–258.
- Capotondi, A., Wittenberg, A.T., Newman, M., Di Lorenzo, E., Yu, J.-Y., Braconnot, P., Cole, J., Dewitte, B., Giese, B., Guilyardi, E., Jin, F.-F., Karnauskas, K., Kirtman, B., Lee, T., Schneider, N., Xue, Y. and Yeh, S.-W. (2015) Understanding ENSO diversity. *Bulletin of the American Meteorological Society*, 96, 921–938.
- ECMWF (2019) ERA5 Climate Reanalysis. Available at: <https://www.ecmwf.int/en/forecasts/datasets/reanalysis-datasets/era5>.
- Finney, D.L., Marsham, J.H., Walker, D.P., Birch, C.E., Woodhams, B.J., Jackson, L.S. and Hardy, S. (2019) The effect of westerlies on east african rainfall and the associated role of tropical cyclones and the madden–julian oscillation. *Quarterly Journal of the Royal Meteorological Society*, 146, 647–664.

- Funk, C., Peterson, P., Landsfeld, M., Pedreros, D., Verdin, J., Shukla, S., Husak, G., Rowland, J., Harrison, L., Hoell, A., et al. (2015) The climate hazards infrared precipitation with stations—a new environmental record for monitoring extremes. *Scientific data*, 2, 1–21.
- Goddard, L. and Graham, N.E. (1999) Importance of the Indian Ocean for simulating rainfall anomalies over eastern and southern Africa. *Journal of Geophysical Research: Atmospheres*, 104, 19099–19116.
- Hirons, L. and Turner, A. (2018) The impact of Indian Ocean mean-state biases in climate models on the representation of the East African short rains. *Journal of Climate*, 31, 6611–6631.
- Kilavi, M., MacLeod, D., Ambani, M., Robbins, J., Dankers, R., Graham, R., Titley, H., Salih, A.A. and Todd, M.C. (2018) Extreme rainfall and flooding over Central Kenya including Nairobi city during the long-rains season 2018: causes, predictability, and potential for early warning and actions. *Atmosphere*, 9, 472.
- Kinuthia, J.H. (1992) Horizontal and vertical structure of the Lake Turkana jet. *Journal of applied meteorology*, 31, 1248–1274.
- Latif, M., Dommengot, D., Dima, M. and Grötzner, A. (1999) The role of Indian Ocean Sea surface temperature in forcing east African rainfall anomalies during December–January 1997/98. *Journal of Climate*, 12, 3497–3504.
- MacLeod, D. (2019) *Seasonal forecast skill over the Greater Horn of Africa: a verification atlas of System 4 and SEAS5 - part1/2*. Reading, UK: ECMWF, Available at: <https://www.ecmwf.int/node/18906>.
- MacLeod, D. and Caminade, C. (2019) The moderate impact of the 2015 el niño over east africa and its representation in seasonal reforecasts. *Journal of Climate*, 32, 7989–8001.
- Mwangi, E., Watterhall, F., Dutra, E., Giuseppe, F. and Pappenbenger, F. (2013) Forecasting droughts in East Africa. *Journal of Hydrology and Earth Sciences*, 10, 10209–10230.
- Nicholson, S. (2016) The Turkana low-level jet: mean climatology and association with regional aridity. *International Journal of Climatology*, 36, 2598–2614.
- Nicholson, S. (2017) Climate and climatic variability of rainfall over eastern Africa. *Reviews of Geophysics*, 55, 590–635.
- de la Poterie, A.S.T., Jjemba, W.E., Singh, R., de Perez, E.C., Costella, C.V. and Arrighi, J. (2018) Understanding the use of 2015–2016 El Niño forecasts in shaping early humanitarian action in eastern and southern Africa. *International Journal of Disaster Risk Reduction*, 30, 81–94.
- Preethi, B., Sabin, T., Adedoyin, J. and Ashok, K. (2015) Impacts of the ENSO Modoki and other tropical indo-Pacific climate-drivers on African rainfall. *Scientific reports*, 5, 16653.
- Rayner, N., Parker, D.E., Horton, E., Folland, C.K., Alexander, L.V., Rowell, D., Kent, E. and Kaplan, A. (2003) Global analyses of sea surface temperature, sea ice, and night marine air temperature since the late nineteenth century. *Journal of Geophysical Research: Atmospheres*, 108, 4407. <https://doi.org/10.1029/2002JD002670>, 2003.
- Rocha, A. and Simmonds, I. (1997) Interannual variability of south-eastern African summer rainfall. Part 1: relationships with air-sea interaction processes. *International Journal of Climatology: A Journal of the Royal Meteorological Society*, 17, 235–265.
- Saji, N., Goswami, B., Vinayachandran, P. and Yamagata, T. (1999) A dipole mode in the tropical Indian Ocean. *Nature*, 401, 360–363.
- Shukla, S., Roberts, J., Hoell, A., Funk, C.C., Robertson, F. and Kirtman, B. (2016) Assessing north American multimodel ensemble (NMME) seasonal forecast skill to assist in the early warning of anomalous hydrometeorological events over East Africa. *Climate Dynamics*, 53, 7411–7427.
- Wainwright, C.M., Finney, D.L., Kilavi, M., Black, E. and Marsham, J. H. (2020) Extreme rainfall in east africa, october 2019–january 2020 and context under future climate change. *Weather*. <https://rmets.onlinelibrary.wiley.com/doi/full/10.1002/wea.3824>.
- Walker, D.P., Birch, C.E., Marsham, J.H., Scaife, A.A., Graham, R.J. and Segele, Z.T. (2019) Skill of dynamical and GHACOF consensus seasonal forecasts of east African rainfall. *Climate Dynamics*, 53, 4911–4935.
- WMO (2020) *Guidance on Operational Practices for Objective Seasonal Forecasting*. Geneva, Switzerland: World Meteorological Organization, Available at: https://library.wmo.int/doc_num.php?explnum_id=10314.
- Yeh, S.-W., Cai, W., Min, S.-K., McPhaden, M.J., Dommengot, D., Dewitte, B., Collins, M., Ashok, K., An, S.-I., Yim, B.-Y. and Kug, J. S. (2018) Enso atmospheric teleconnections and their response to greenhouse gas forcing. *Reviews of Geophysics*, 56, 185–206.
- Yeh, S.-W., Kug, J.-S., Dewitte, B., Kwon, M.-H., Kirtman, B.P. and Jin, F.-F. (2009) El Niño in a changing climate. *Nature*, 461, 511–514.
- Yu, J.-Y., Zou, Y., Kim, S.T. and Lee, T. (2012) The changing impact of El Niño on US winter temperatures. *Geophysical Research Letters*, 39, L15702. <https://doi.org/10.1029/2012GL052483>.

SUPPORTING INFORMATION

Additional supporting information may be found online in the Supporting Information section at the end of this article.

How to cite this article: MacLeod D, Graham R, O'Reilly C, Otieno G, Todd M. Causal pathways linking different flavours of ENSO with the Greater Horn of Africa short rains. *Atmos Sci Lett*. 2021;22: e1015. <https://doi.org/10.1002/asl.1015>